GDCh Research Article Angewandte International Edition Chemie www.angewandte.org

How to cite: *Angew. Chem. Int. Ed.* **2025**, *64*, e202511678
doi.org/10.1002/anie.202511678

Photochemistry

Isotope Engineering of Tetraphenylethylene: Aggregate-Dependent Enhancement of Luminescence Efficiency

Siwei Zhang[+], Fulong Ma[+], Jinhui Jiang, Bo Wu, Junyi Gong, Guang Xu, Chao Li, Tengteng Chen, Ryan T. K. Kwok, Jacky W. Y. Lam,* Zheng Zhao,* and Ben Zhong Tang**

Abstract: Aggregation-induced emission (AIE) luminogens, exemplified by tetraphenylethylene (TPE), exhibit enhanced fluorescence in aggregated states and have promising applications in display, photodetectors, fluorescent probes, bioimaging, and biomedicine. This study investigates the influence of varying degrees of deuteration on the photophysical properties of TPE across different aggregation states. Through the synthesis of partially and fully deuterated TPE derivatives (TPE-5d, TPE-10d, and TPE-20d), combined with steady-state fluorescence spectroscopy, time-resolved fluorescence measurements, transient absorption spectroscopy, and density functional theory (DFT) calculations, we elucidate the dual role of deuteration in modulating nonradiative decay pathways. In loosely packed nanoaggregates, increased deuteration enhances photoluminescence quantum yields (PLQY) and extends fluorescence lifetimes by reducing internal conversion rates. Conversely, in tightly packed crystalline states, deuteration leads to decreased PLQY and shortened lifetimes, attributable to the Duschinsky rotation effect (DRE), which enhances inter-mode coupling and internal conversion. Additionally, deuteration significantly prolongs the operational lifetime of blue organic light-emitting diode (OLED) devices, doubling the device lifespan in TPE-20d compared to TPE. This work underscores the necessity of evaluating structure–property relationships at the aggregate level, rather than solely at the molecular level, to fully comprehend and optimize AIE phenomena. These findings highlight the potential of isotope engineering in designing durable and efficient AIE luminogens for applications in optoelectronics and bioimaging.

Introduction

Aggregation-induced emission (AIE) luminogens have garnered significant attention both in organic and inorganic materials[1,2] due to their unique photophysical properties,[3,4] wherein molecules exhibit enhanced fluorescence upon aggregation and have promising applications in display,[5] photodetectors,[6] fluorescent probes,[7] bioimaging,[8] and biomedicine.[9] Tetraphenylethylene (TPE) is a prototypical AIEgen, renowned for its facile synthesis and widespread application as a molecular building block in various optoelectronic devices and bioimaging probes.[10–12] TPE belongs to aggregation-activated fluorescence,[13] meaning that while TPE molecules possess intrinsic luminescence capabilities, their emission at room temperature is too weak to be detectable due to molecular motion. The restriction of intramolecular motions (RIM)[14] upon aggregation significantly enhances the fluorescence intensity of TPE.[15]

The excited-state dynamics of TPE are inherently complex, involving a network of intramolecular conformational changes and potential side reactions.[15,16] Upon photoexcitation, TPE undergoes significant molecular reconfigurations:

[*] Dr. S. Zhang[+], Dr. F. Ma[+], Dr. J. Jiang, Prof. R. T. K. Kwok, Prof. J. W. Y. Lam, Prof. B. Z. Tang
Department of Chemistry, Hong Kong Branch of Chinese National Engineering Research Center for Tissue Restoration and Reconstruction, Division of Life Science and State Key Laboratory of Molecular Neuroscience, The Hong Kong University of Science and Technology, Kowloon, Hong Kong 999077, China
E-mail: chjacky@ust.hk
tangbenz@ust.hk

Prof. B. Wu
School of Environmental and Chemical Engineering, Wuyi University, Jiangmen, Guangdong 529020, China
E-mail: wubo@wyu.edu.cn

Prof. J. Gong
Faculty of Chemistry, Shenzhen MSU-BIT University, Longgang District, Shenzhen, Guangdong 518172, China

G. Xu, Prof. Z. Zhao, Prof. B. Z. Tang
Guangdong Basic Research Center of Excellence for Aggregate Science, School of Science and Engineering, Shenzhen Institute of Aggregate Science and Technology, The Chinese University of Hong Kong (CUHK-Shenzhen), Shenzhen, Guangdong 518172, China
E-mail: zhaozheng@cuhk.edu.cn

Dr. C. Li, Prof. T. Chen
Department of Chemistry, The Hong Kong University of Science and Technology, Clear Water Bay, Kowloon, Hong Kong 999077, China

[+] Both authors contributed equally to this work.

Additional supporting information can be found online in the Supporting Information section

each of the four peripheral phenyl rings can twist nearly freely about the central C═C bond. These large-amplitude torsions open up conical intersections (CIs) with the ground state, leading to ultrafast internal conversion (IC) on the sub-picosecond timescale and quenching fluorescence.[17] In addition to ring rotation, the central double bond itself can rotate or bend, further supplying a low-energy pathway to nonradiative decay via another CI seam. These motions lead to the formation of highly nonradiative decay pathways, which are effectively suppressed in the aggregated state due to steric hindrance and restricted molecular freedom. Additionally, secondary processes such as photocyclization can occur, contributing to photobleaching and further complicating the excited-state landscape. The interplay between these dynamic molecular motions and the surrounding environment dictates the efficiency of fluorescence emission, making TPE an ideal candidate for studying the fundamental mechanisms underpinning AIE.[18] Extensive studies utilizing various spectroscopic techniques, including time-resolved fluorescence spectroscopy and transient absorption spectroscopy, have been employed to unravel these complex excited-state behaviors.[16] However, the precise role of different intramolecular motions and their suppression in various aggregated states remains an area of active investigation.

Isotopic substitution, particularly deuteration, has emerged as a powerful tool for probing excited-state decay processes.[19–22] In conventional fluorophores, deuteration typically results in a decrease in nonradiative decay rates without significantly altering radiative rates, thereby enhancing photoluminescence quantum yields (PLQY).[19,23] This effect is explained by the reduced vibrational frequencies of C─D bonds compared to C─H bonds, leading to higher Huang–Rhys factors and decreased internal conversion rates (KIC) within the displaced harmonic oscillator model.[24,25] However, if the nonradiative transition of the fluorophores is mainly intersystem crossing (ISC), such as in polycyclic aromatic hydrocarbons or anthracene, the effect of deuteration on KIC is limited, but it changes the zero-point energy difference and the vibrational energy level spacing so that the vibration-electron coupling of the S1/T1 state in some medium- and low-frequency modes is enhanced, which promotes KISC and causes a decrease in PLQY.[19,26] Furthermore, in flexible AIEgens like TPE, the situation is more nuanced due to the significant mixing between low-frequency vibrational modes and the associated Duschinsky rotation effect (DRE), which can potentially increase KIC.[27] Deuteration in such systems introduces two competing effects: it increases the Huang–Rhys factor, thereby reducing KIC, while simultaneously strengthening the DRE, enhancing inter-mode coupling, and increasing KIC. Understanding the competition between these opposing influences is crucial for elucidating the impact of deuteration on the photophysical properties of organic molecules and for the rational design of highly efficient AIE luminogens.

This study aims to investigate the dual effects of deuteration on the photophysical properties of TPE in different aggregation states. By synthesizing partially and fully deuterated TPE derivatives (TPE-5d, TPE-10d, and TPE-20d) and employing a combination of experimental techniques and theoretical calculations, we explore how deuteration influences intramolecular motions and nonradiative decay pathways in both solution and aggregated/crystalline states. Additionally, we assess the practical implications of deuteration in enhancing the operational lifetime of organic light-emitting diodes (OLEDs), thereby bridging fundamental mechanistic insights with device performance. This comprehensive approach not only advances our understanding of the impact of deuteration on the photophysical properties of molecules but also demonstrates the potential of isotope engineering in developing durable and efficient luminescent materials for advanced optoelectronic applications.

Results and Discussion

The synthesis of deuterated TPE derivatives (TPE-5d, TPE-10d, and TPE-20d) was successfully achieved via selective deuteration of the phenyl rings (Figure S1). The structures of the synthesized compounds were confirmed by ^{1}H nuclear magnetic resonance (NMR), ^{13}C NMR, and high-resolution mass spectrometry (Figures S2–S12). Single-crystal X-ray diffraction studies (Figures 1a and S13)[28–31] revealed that deuteration induced only minor changes in the central C═C bond length, from 1.361 Å in TPE to 1.346 Å in TPE-5d and TPE-10d and 1.351 Å in TPE-20d. Additionally, dihedral angles between adjacent phenyl rings remained similar postdeuteration, indicating negligible alterations in molecular conformation (Tables S1–S4). X-ray diffraction (XRD) patterns of deuterated derivatives confirmed that the crystalline packing remained similar to nondeuterated TPE, with only slight shifts in diffraction peaks indicating marginally tighter packing in TPE-20d (Figure S14). There were no significant changes in the absorption spectra (Figure S15).

Raman and Fourier-transform infrared (FTIR) spectroscopy were employed to investigate the vibrational modes of deuterated TPE derivatives (Figure 1b,c). Deuteration resulted in the weakening of the C─H stretching vibrations around 3100 cm^{-1} and the enhancement of C─D stretching modes near 2300 cm^{-1}. The Huang–Rhys factor, $\boldsymbol{S}$, is approximated by $\boldsymbol{S} \approx \Delta\boldsymbol{Q}^2/(2\boldsymbol{hw})$, where $\Delta\boldsymbol{Q}$ represents the nuclear displacement during excitation and $\boldsymbol{hw}$ is the vibrational energy quantum. Since deuterium is heavier than hydrogen, replacing C─H with C─D lowers $\boldsymbol{hw}$; if $\Delta\boldsymbol{Q}$ remains nearly constant, $\boldsymbol{S}$ increases, decreasing KIC.

Based on the observed effects of deuteration on the vibrational modes of TPE molecules, we further investigated the photophysical properties of TPE and its deuterated derivatives in various states. In dilute solution (1×10^{-5} M in tetrahydrofuran (THF)), no detectable photoluminescence (PL) spectrum was observed at room temperature, consistent with nonemissive behavior resulting from dynamic quenching due to intramolecular motions.[14,32] Upon the formation of nano-sized aggregates in THF-water mixtures (concentration: 1×10^{-5} M, THF:H_2O = 1:9, labeled as the nano-aggregated state), deuteration led to notable changes in the PL characteristics. As the degree of deuteration increased from TPE to TPE-20d, the PL emission peak remained around 470 nm (Figure S16), while fluorescence lifetimes (τ)

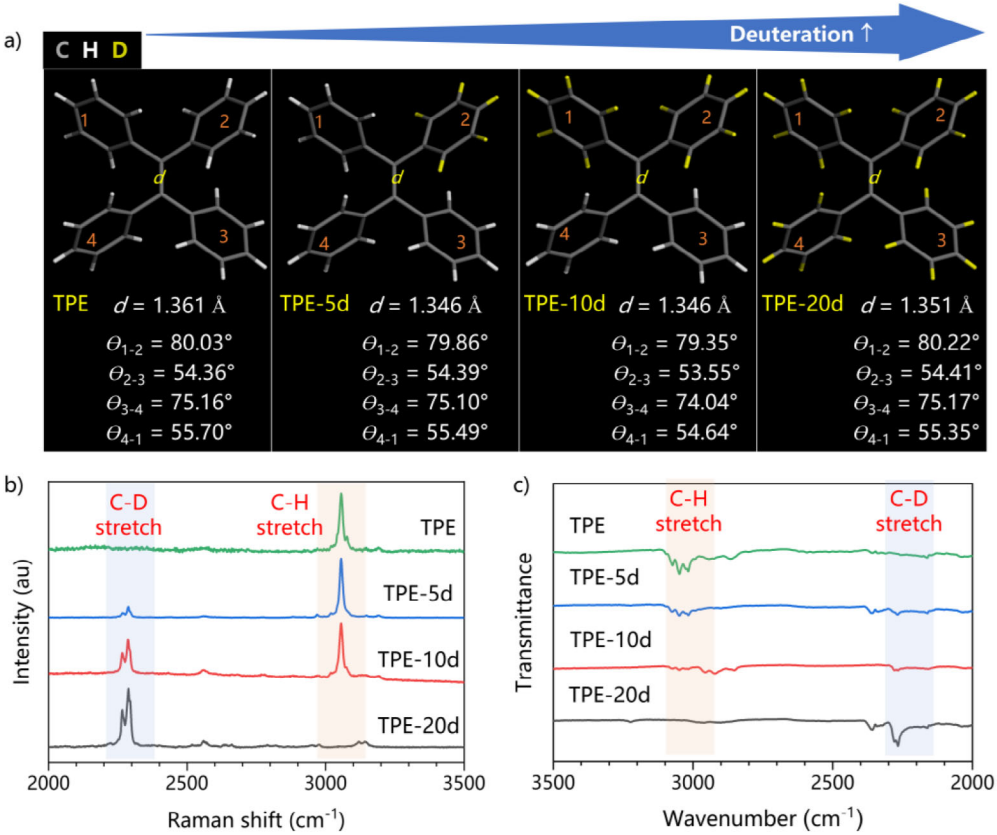

Figure 1. Structural and spectroscopic characterization of deuterated TPE derivatives (TPE-5d, TPE-10d, and TPE-20d). a) Single-crystal structure of TPE and deuterated derivatives, highlighting minor shifts in C=C bond lengths and dihedral angles. b) Raman and c) FTIR spectra demonstrating vibrational mode changes due to deuteration in crystalline form.

Table 1: Photophysical property of TPE and deuterated TPE derivatives in nano-aggregate and crystalline states.

Samples		PL peak (nm)	τ (ns)	PLQY (%)	K_r ($\times 10^7$ s^{-1})	K_{nr} ($\times 10^7$ s^{-1})
Nano-aggregate state	TPE	472	3.62	21.12	5.83	21.79
	TPE-5d	471	3.80	21.52	5.66	20.65
	TPE-10d	471	4.05	22.86	5.64	19.05
	TPE-20d	471	4.22	24.40	5.78	17.91
Crystalline state	TPE	447	1.56	24.04	15.41	48.69
	TPE-5d	445	1.45	24.10	16.62	52.34
	TPE-10d	444	1.38	22.56	16.35	56.12
	TPE-20d	442	1.23	20.28	16.49	64.81

extended from 3.62 ns in TPE to 4.22 ns in TPE-20d, and PLQY increased from 21.12% to 24.40% (Table 1). Based on these measurements, we calculated the radiative transition constant ($K_r = PLQY/\tau$) and the nonradiative transition constant ($K_{nr} = (1 - PLQY)/\tau$). While K_r exhibited minimal variation with deuteration, K_{nr} decreased as the degree of deuteration increased, indicating that the positive effects of deuteration prevail in the nano-aggregate state. These observations suggest that deuteration reduces nonradiative decay rates by suppressing internal conversion pathways, thereby enhancing fluorescence efficiency in nano-aggregated state.

Conversely, in crystalline states (Figure S17), the PL peak exhibits a blue shift relative to nano-aggregated states due to conformational rigidification; the conical intersection (CI) and excited-state minimum are not accessible energetically.[33] Deuterated TPE derivatives demonstrate shortened τ and diminished PLQY. Specifically, τ decreases from 1.56 ns in TPE to 1.23 ns in TPE-20d, and PLQY declines from 24.04% to 20.28%. In other words, as the degree of deuteration increases, the K_{nr} in crystalline states progressively intensifies. This negative isotope effect in rigid, tightly packed crystals suggests an enhancement of K_{IC}, likely attributable to the DRE facilitated by deuteration, which promotes mode mixing and nonradiative decay processes.

To further investigate how deuteration and different aggregation states affect the photophysical properties of TPE, we performed comprehensive theoretical calculations. First,

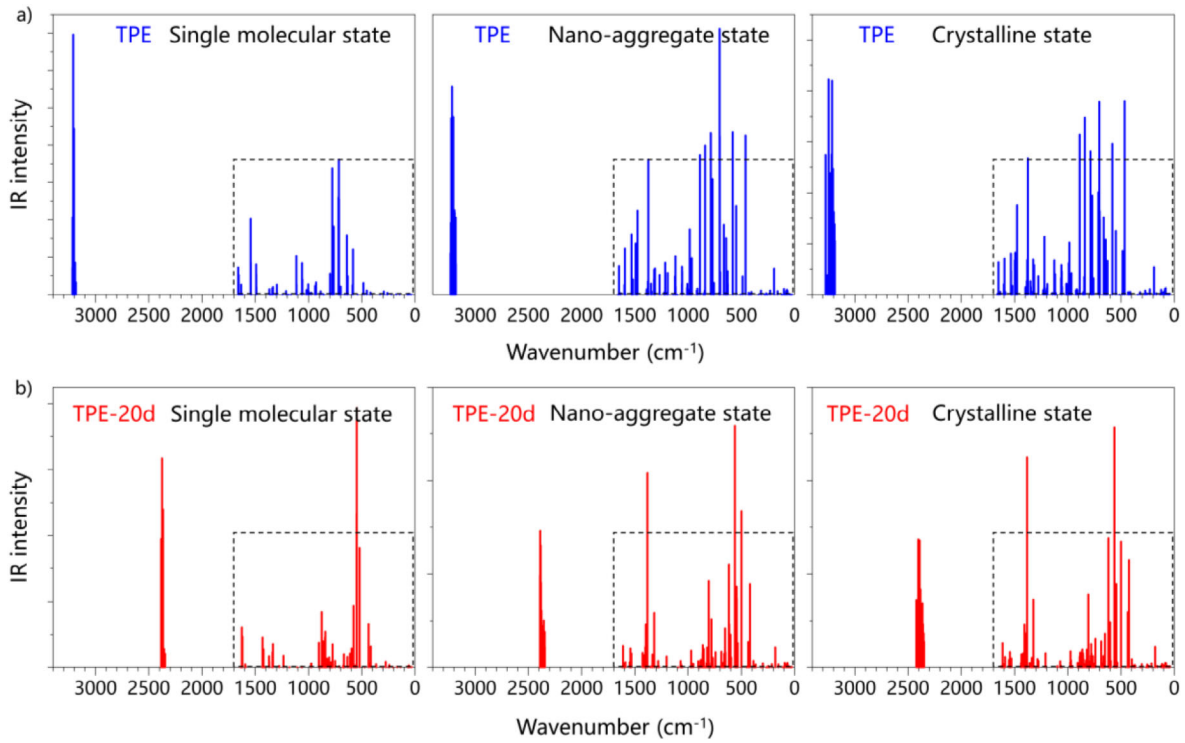

Figure 2. Theoretical calculation of vibration (IR) spectra of a) TPE and b) TPE-20d at single molecular state, nano-aggregate state, and crystalline state.

we computed the IR spectra of various deuterated derivatives of TPE in the single-molecule state. As shown in Figure S20, the characteristic C─H stretching vibration at approximately 3200 cm^{-1} in pristine TPE is replaced by a C─D stretching vibration around 2300 cm^{-1} with increasing degrees of deuteration. This clear shift in vibrational frequency agrees well with our earlier experimental results and confirms the expected isotopic substitution effect. In the low-frequency region (lower than 1500 cm^{-1}), deuteration significantly alters the vibrational landscape. Notably, the impact is not only dependent on the overall degree of deuteration but also on the specific locations and symmetry of the deuterated sites. As illustrated in Figure S21, several vibrational bands greatly changed after deuteration—primarily corresponding to modified C─H/D stretching modes and benzene ring contraction vibrations. This proliferation of modes likely reflects changes in the vibrational coupling and symmetry of the molecule upon deuteration.

The influence of aggregation on the IR spectra is also quite striking (the method for constructing the nano-aggregate state is shown in Figure S22). Figures 2 and S23 compare the spectra of TPE and its fully deuterated derivative, TPE-20d, in nano-aggregate and crystalline states. For TPE, transitioning from a single-molecule state to a nano-aggregate state leads to a noticeable increase in the number of low-frequency vibrational modes. In the crystalline state, these additional modes are further augmented, indicating that aggregation promotes the activation of new low-frequency vibrational transitions. Furthermore, TPE-20d exhibits a similar trend; however, the number of low-frequency modes increases even more markedly than in TPE. This suggests that deuteration intensifies the aggregation-induced emergence of low-frequency vibrational modes, thereby potentially enhancing the mixing between low-frequency vibrational modes and the associated DRE.

We systematically examined the effects of aggregation state and deuteration on the vibrational-electron coupling in TPE derivatives by probing both Huang–Rhys factors and reorganization energies. As shown in Figure 3 and Table S6, for TPE, in the nano-aggregate state, the vibrational modes extend from approximately 22 cm^{-1} to about 122 cm^{-1}, with the corresponding Huang–Rhys factors increasing from roughly 9.4 to nearly 364.0. In contrast, in the crystalline state, the frequency distribution primarily spans the range of 43–67 cm^{-1}, and the Huang–Rhys factors drop to a lower range between approximately 7.6 and 67.7. This suggests that the ordered crystalline environment restricts the vibrational mobility, thereby weakening the electron-phonon coupling.

For the TPE-20d, the vibrational mode frequencies in the nano-aggregate state are similar to those of TPE, ranging from about 22 cm^{-1} to around 112 cm^{-1}. However, the corresponding Huang–Rhys factors are generally higher, between approximately 12.8 and 399.6, indicating that deuteration enhances the vibrational-electron coupling. The crystalline state for TPE-20d exhibits frequency distribution from 42 to 58 cm^{-1} and displays a noticeable fluctuation in Huang–Rhys factors (7.8–76.3). These observations indicate that both the molecular aggregation state and deuteration critically modulate the vibrational characteristics—deuteration not only shifts individual vibrational frequencies

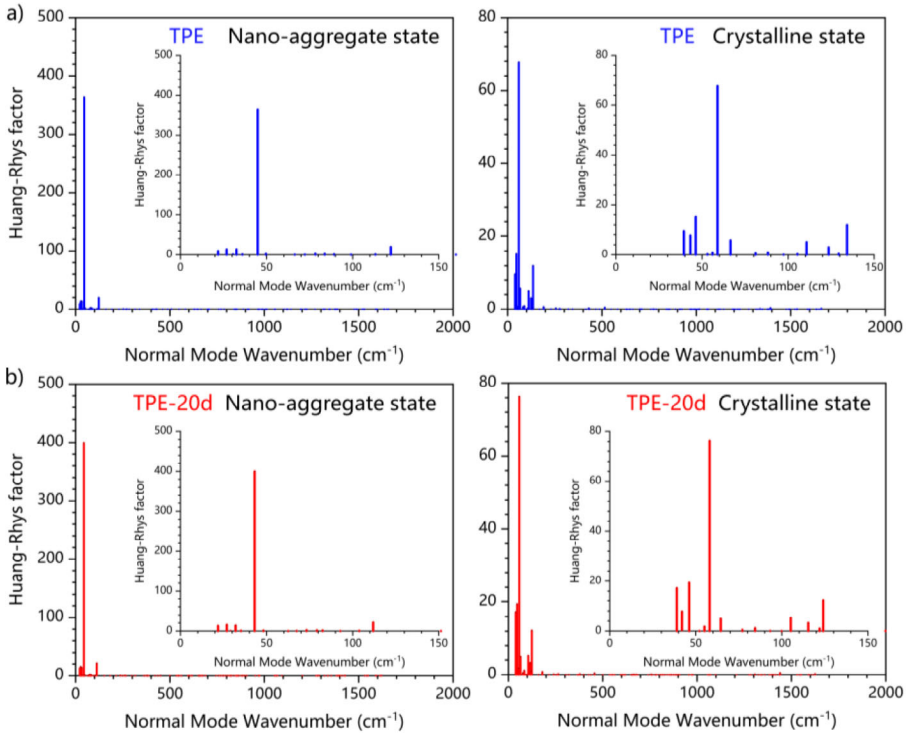

Figure 3. Calculated Huang–Rhys factor versus the normal-mode frequencies of a) TPE and b) TPE-20d at nano-aggregate state and crystalline state.

(for example, the transition from C─H to C─D stretching) but also fundamentally alters the vibronic coupling behavior, thereby potentially affecting the overall photophysical properties.

Complementary insights are provided by the analysis of reorganization energies, which were decomposed into contributions from bond lengths, bond angles, and dihedral angles. As shown in Figure 4, for the TPE sample, compared to the nano-aggregate state, the contribution from low-frequency vibrational modes becomes more pronounced in the crystalline state, resulting in a significant change in the overall distribution of reorganization energy. In the nano-aggregate state, the reorganization energy is mainly constituted by changes in dihedral angles (68.39%), indicating that in a relatively loose aggregated system, high-frequency vibrations (such as bond stretching and benzene ring deformations) dominate. However, when the molecules transition into the crystalline state, the molecular packing becomes more regular and compact, which restricts high-frequency vibrations while relatively enhancing the influence of low-frequency vibrational modes, with the contribution from dihedral angles being reduced. TPE-20d exhibits a similar trend, compared to the nano-aggregate state, molecules in the crystalline state rely more on low-frequency vibrational modes for energy relaxation, particularly involving torsional motions related to dihedral angles. This change in aggregation state not only alters the overall distribution of reorganization energy but also underscores the crucial role of the molecular environment in governing energy relaxation processes.

Figure 5 provides deeper insight into the decay pathways by demonstrating the DRE. The contour maps of the Duschinsky rotation matrix for the lowest 130 normal modes reveal notable differences between the nano-aggregate and crystalline states. In the nano-aggregate state, the Duschinsky rotation matrix elements remain closer to their ideal values, while in the crystalline state, there is a more pronounced deviation—evidenced by an increase in off-diagonal elements. These deviations, particularly in low-frequency modes, point to a significant role for low-frequency twisting motions in nonradiative decay. Especially TPE-20d in the crystalline state shows even more off-diagonal contributions, suggesting that the ordered, dense molecular packing combined with deuteration amplifies multiple low-frequency twisting motions. This enhancement likely contributes considerably to the nonradiative deactivation of excitons. The theoretical calculation of the nonradiative transition rate is also consistent with the experimental results (Tables S7 and S8), which once again proves the rationality of the above calculation.

The theoretical calculations confirm that aggregation significantly influences the low-frequency vibrational modes of TPE and its deuterated derivative. In the crystalline state, which features tighter molecular packing, the coupling between low-frequency vibrational modes and the excited-state low-frequency modes is markedly intensified. Additionally, deuteration further amplifies the DRE effect, thereby activating more nonradiative transitions.

Finally, we investigated the impact of deuteration on the stability of the materials. Thermogravimetric analysis (TGA) and differential scanning calorimetry (DSC) were conducted on materials with varying degrees of deuteration (Figure S24 and Table S9). The results revealed that deuteration had negligible effects on the thermal stability of the materials. This

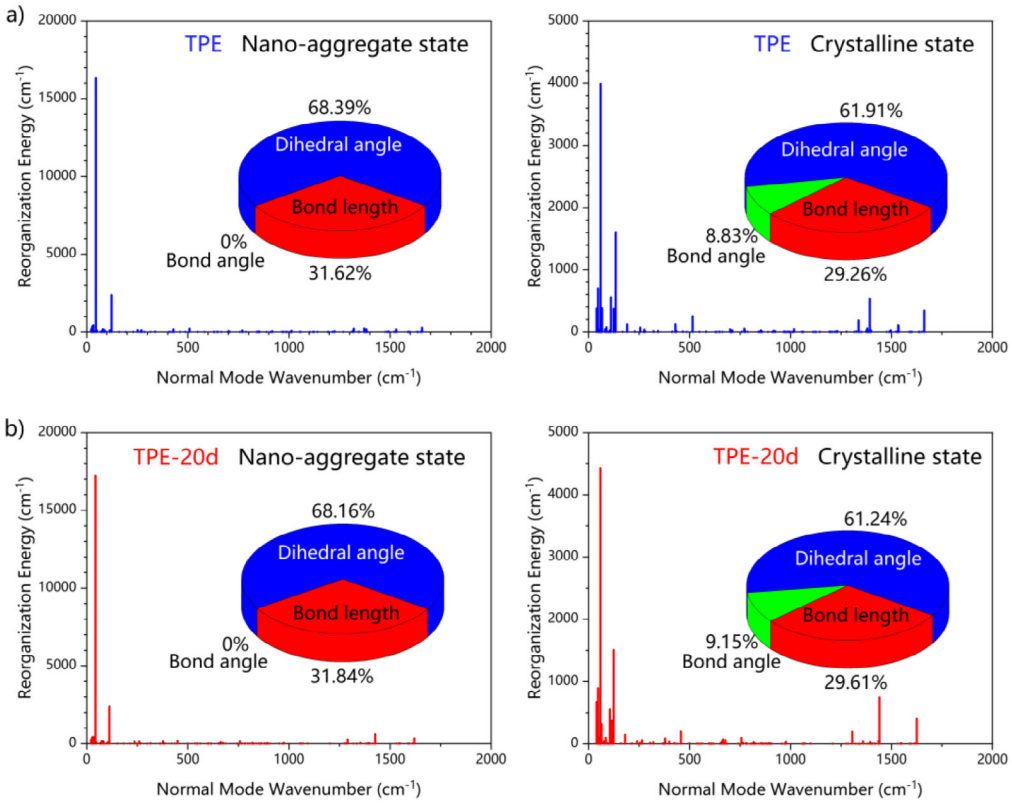

Figure 4. Calculated reorganization energies versus the normal-mode frequencies of a) TPE and b) TPE-20d at nano-aggregate state and crystalline state. Inset: Contributions to the total reorganization energies from bond length, bond angle, and dihedral angle.

observation is understandable, as the increase in molecular weight due to deuteration is minimal relative to the entire molecular system, and thermal stability is directly related to molecular weight. Consequently, deuteration does not significantly influence the thermal decomposition temperatures of the materials.

The photostability tests under continuous irradiation reveal that the TPE-20d exhibits a markedly slower decay in photoluminescence intensity compared with TPE, indicating that TPE-20d resists photodegradation more effectively (Figure S25). The femtosecond transient absorption proves that the photo-cyclized behavior of TPE is limited in the film state (Figures S26 and S27). However, the electrochemical stability assessments show that TPE-20d demonstrates a similar current response with TPE across a broader potential range. This behavior suggests that the deuterated derivative undergoes less effect on electrochemical degradation.

Subsequently, we fabricated undoped organic light-emitting diode (OLED) devices using TPE as the emissive layer (Figure 6 and Table S10). The device structure is illustrated as follows: ITO/NPB (40 nm)/TPE (20 nm)/TPBi (40 nm)/LiQ (2 nm)/Al (NPB: N^4,N^4-di(naphthalen-1-yl)-N^4,N^4-diphenyl-[1,1-biphenyl]-4,4-diamine; TPBi: 2,2′,2″-(1,3,5-benzinetriyl)-tris(1-phenyl-1-*H*-benzimidazole); LiQ: 8-quinolinolato lithium). Under identical device architectures, the current–voltage (*J*–*V*) curves, external quantum yields (EQE), and electroluminescence (EL) spectra of TPE, TPE-5d, and TPE-20d exhibited comparable performances. However, the operational lifetimes of the devices significantly increased with the degree of deuteration. Specifically, the lifetime of the TPE-20d-based device was extended 10-fold compared to that of the nondeuterated TPE-based device. This enhancement in the operational lifetime of deuterated TPE derivatives is primarily attributed to their reduced susceptibility to photodegradation mechanisms.[34] Deuteration strengthens the C─D bonds relative to C─H bonds (≈0.0607 eV), thereby decreasing the likelihood of C─D bond cleavage under the high-energy excitations typical of blue-emitting materials.[35] This bond stabilization mitigates degradation pathways such as direct photolysis, triplet state-induced reactions, and oxygen-mediated oxidative processes.[36] Consequently, deuteration significantly enhances material stability, leading to prolonged operational lifetimes of OLED devices.

Conclusion

This study systematically investigates the influence of deuteration on the photophysical properties of TPE across different aggregation states through both experimental measurements and theoretical calculations. In nano-sized aggregates, enhanced deuteration suppresses nonradiative decay pathways, resulting in increased fluorescence quantum yields (PLQY) and extended fluorescence lifetimes. Conversely, in crystalline states, deuteration augments internal conversion rates via the Duschinsky rotation effect (DRE), leading to decreased PLQY and shortened lifetimes. Additionally,

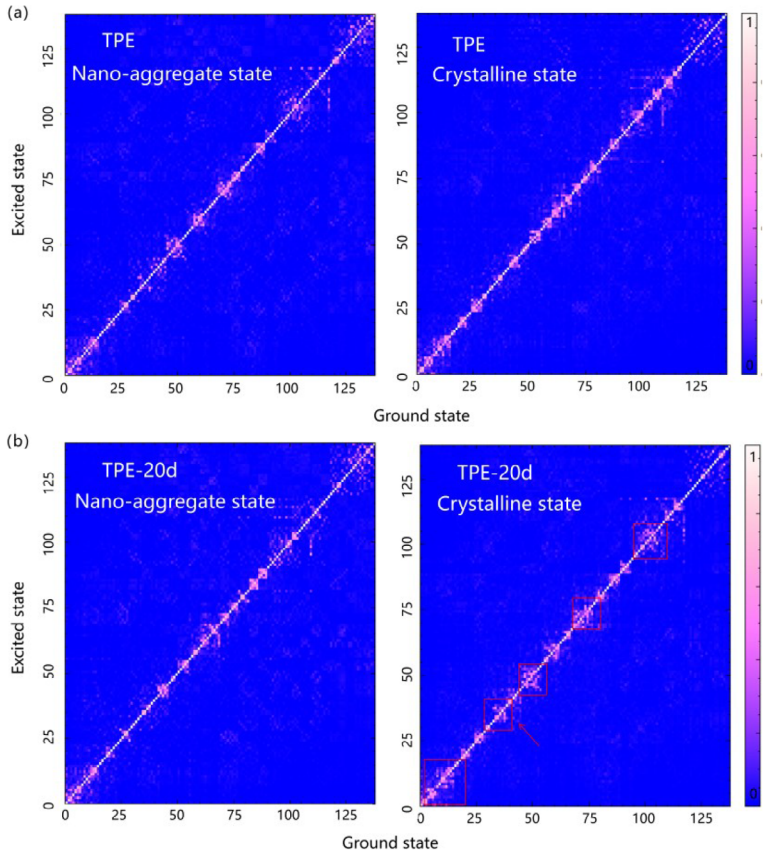

Figure 5. Contour maps of the Duschinsky rotation matrix of a) TPE and b) TPE-20d at nano-aggregate state and crystalline state.

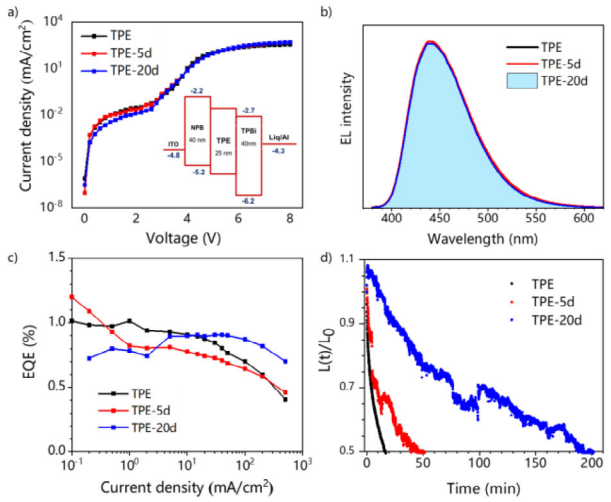

Figure 6. a) The *J*–*V* characteristics (inset: OLED device structure). b) The electroluminescence (EL) spectrum at 5 V. c) External quantum efficiency (EQE) and d) lifetime of the OLED-based TPE, TPE-5d, and TPE-20d as emitters.

deuteration significantly prolongs the operational lifetime of OLED devices, doubling the device lifespan in deuterated TPE-20d compared to nondeuterated TPE. These findings elucidate the dual role of deuteration in modulating AIE mechanisms and underscore the critical importance of the molecular environment in determining photophysical behavior. The demonstrated extension of OLED device lifetimes further highlights the practical significance of isotope engineering in the design of efficient and durable AIE luminogens for advanced optoelectronic applications.

Acknowledgements

This project is supported by the National Key Research and Development Program of China (2023YFB3810001), the NSFC (52333007 and 52273197), the Shenzhen Key Laboratory of Functional Aggregate Materials (ZDSYS20211021111400001), the Science Technology Innovation Commission of Shenzhen Municipality (GJHZ20210705141810031, KQTD20210811090142053, and JCYJ20220818103007014), the Innovation and Technology Commission (ITC-CNERC14SC01), and the Science and Technology Program of Guangzhou, China (2023A04J0069). The authors thank the Materials Characterization and Preparation Center, the Chinese University of Hong Kong, Shenzhen, for the material characterization.

Conflict of Interests

The authors declare no conflict of interest.

Data Availability Statement

The data that support the findings of this study are available in the Supporting Information of this article.

Keywords: Aggregation-induced emission • Deuteration • OLED stability • Photophysical properties • Tetraphenylethylene

[1] Y. Wang, J. Wang, S. Zhang, N. Y. B. Tang, X. Ou, J. Jiang, F. Ma, P. Alam, Z. Qiu, W. J. Wang, Z. Zhao, J. W. Y. Lam, B. Z. Tang, *ACS Nano* **2025**, *19*, 25042–25051.
[2] S. Zhang, F. Ma, J. Jiang, Z. Wang, R. T. K. Kwok, Z. Qiu, Z. Zhao, J. W. Y. Lam, B. Z. Tang, *Angew. Chem. Int. Ed.* **2024**, *63*, e202408586.
[3] Q. Peng, Z. Shuai, *Aggregate* **2021**, *2*, e91.
[4] Z. Shuai, Q. Sun, J. Ren, T. Jiang, W. Li, *Aggregate* **2025**, *6*, e70013.
[5] Z. L. Gong, X. F. Zhu, Z. H. Zhou, S. W. Zhang, D. Yang, B. Zhao, Y. P. Zhang, J. P. Deng, Y. X. Cheng, Y. X. Zheng, S. Q. Zang, H. Kuang, P. F. Duan, M. J. Yuan, C. F. Chen, Y. S. Zhao, Y. W. Zhong, B. Z. Tang, M. H. Liu, *Sci. China Chem.* **2021**, *64*, 2060–2104.
[6] S. Zhang, Z. Li, J. Li, B. Wang, F. Chen, X. Li, S. Liu, J. W. Y. Lam, G. Xing, J. Li, Z. Zhao, F. Kang, G. Wei, B. Z. Tang, *Aggregate* **2023**, *4*, e345.
[7] Y. B. Yu, S. W. Zhang, J. H. Jiang, F. L. Ma, R. Wang, T. H. Huang, J. W. Zhao, C. He, G. D. Wei, *Adv. Sens. Res.* **2023**, *2*, 2300027.
[8] R. Zhang, P. Shen, Y. Xiong, T. Wu, G. Wang, Y. Wang, L. Zhang, H. Yang, W. He, J. Du, X. Wei, S. Zhang, Z. Qiu, W. Zhang, Z. Zhao, B. Z. Tang, *Natl. Sci. Rev.* **2024**, *11*, nwad286.
[9] S. Zhang, J. Wang, Z. Wang, M. Shao, C. Zhang, X. Chen, J. Sun, R. T. K. Kwok, J. W. Y. Lam, B. Z. Tang, *J. Mater. Chem. B* **2024**, *12*, 8349–8356.
[10] Z. Zhao, J. W. Y. Lam, B. Z. Tang, *J. Mater. Chem.* **2012**, *22*, 23726-23740.
[11] Y. Yin, Q. Guan, Z. Chen, D. D. Deng, S. Liu, Y. Sun, S. H. Liu, *Sci. Adv.* **2024**, *10*, eadk5444.
[12] Z. Chen, H. Qin, Y. Yin, D. D. Deng, S. Y. Qin, N. Li, K. Wang, Y. Sun, *Chem. Eur. J.* **2023**, *29*, e202203797.
[13] F. Ma, S. Zhang, J. Jiang, Y. Liu, J. Sun, J. W. Y. Lam, Z. Zhao, B. Z. Tang, *Adv. Mater.* **2025**, *37*, e2414188.
[14] N. L. Leung, N. Xie, W. Yuan, Y. Liu, Q. Wu, Q. Peng, Q. Miao, J. W. Lam, B. Z. Tang, *Chemistry* **2014**, *20*, 15349–15353.
[15] H. Zhang, B. Z. Tang, *JACS Au* **2021**, *1*, 1805–1814.
[16] Y. Cai, L. Du, K. Samedov, X. Gu, F. Qi, H. H. Y. Sung, B. O. Patrick, Z. Yan, X. Jiang, H. Zhang, J. W. Y. Lam, I. D. Williams, D. L. Phillips, A. Qin, B. Z. Tang, *Chem. Sci.* **2018**, *9*, 4662–4670.
[17] Y. P. Sun, M. A. Fox, *J. Am. Chem. Soc.* **1993**, *115*, 747–750.
[18] S. Dellonte, G. Marconi, S. Monti, *J. Photochem.* **1987**, *39*, 33–40.
[19] V. L. Ermolaev, *Opt. Spectrosc.* **2016**, *121*, 567–584.
[20] N. Notsuka, R. Kabe, K. Goushi, C. Adachi, *Adv. Funct. Mater.* **2017**, 27.
[21] T. Huang, Q. Wang, H. Zhang, Y. Zhang, G. Zhan, D. Zhang, L. Duan, *Nat. Photonics* **2024**, *18*, 516–523
[22] M. Yuan, F. Ma, X. Dai, L. Chen, F. Zhai, L. He, M. Zhang, J. Chen, J. Shu, X. Wang, X. Wang, Y. Zhang, X. Fu, Z. Li, C. Guo, L. Chen, Z. Chai, S. Wang, *Angew. Chem. Int. Ed.* **2021**, *60*, 21250–21255 *Angew. Chem.* **2021**, *133*, 21420–21425.
[23] F. Ma, Q. Jia, Z. Deng, B. Wang, S. Zhang, J. Jiang, G. Xing, Z. Wang, Z. Qiu, Z. Zhao, B. Z. Tang, *ACS Nano* **2024**, *18*, 9431–9442.
[24] K. Mishra, Z. Wu, C. Erker, K. Mullen, T. Basche, *Chem. Sci.* **2024**, *16*, 90–97.
[25] J. B. Grimm, L. Xie, J. C. Casler, R. Patel, A. N. Tkachuk, N. Falco, H. Choi, J. Lippincott-Schwartz, T. A. Brown, B. S. Glick, Z. Liu, L. D. Lavis, *JACS Au* **2021**, *1*, 690–696.
[26] L. Li, J. Jakowski, C. Do, K. Hong, *Macromolecules* **2021**, *54*, 3555–3584.
[27] T. Zhang, Q. Peng, C. Quan, H. Nie, Y. Niu, Y. Xie, Z. Zhao, B. Z. Tang, Z. Shuai, *Chem. Sci.* **2016**, *7*, 5573–5580.
[28] Cambridge Crystallographic Data Centre Database. Deposition Number: 2430766, https://www.ccdc.cam.ac.uk/structures/Search?ccdc=2430766.
[29] Deposition Number: 2430765, https://www.ccdc.cam.ac.uk/structures/Search?access=referee&ccdc=2430765&Author=Siwei+Zhang.
[30] Deposition Number: 2429083, https://www.ccdc.cam.ac.uk/structures/Search?access=referee&ccdc=2429083&Author=Siwei+Zhang.
[31] Deposition Number: 2429081, https://www.ccdc.cam.ac.uk/structures/Search?ccdc=2429081.
[32] J. K. Liu, H. K. Zhang, L. R. Hu, J. Wang, J. W. Y. Lam, L. Blancafort, B. Z. Tang, *J. Am. Chem. Soc.* **2022**, *144*, 7901–7910.
[33] Z. Zhao, H. Zhang, J. W. Y. Lam, B. Z. Tang, *Angew. Chem. Int. Ed.* **2020**, *59*, 9888–9907.
[34] X. Liu, H. Popli, O. Kwon, H. Malissa, X. Pan, B. Park, B. Choi, S. Kim, E. Ehrenfreund, C. Boehme, Z. V. Vardeny, *Adv. Mater.* **2020**, *32*, e2004421.
[35] J. Yao, S.-C. Dong, B. S. T. Tam, C. W. Tang, *ACS Appl. Mater. Interfaces* **2023**, *15*, 7255–7262.
[36] X. Liu, C.-Y. Chan, F. Mathevet, M. Mamada, Y. Tsuchiya, Y.-T. Lee, H. Nakanotani, S. Kobayashi, M. Shiochi, C. Adachi, *Small Sci.* **2021**, *1*, 2000057.

Manuscript received: May 28, 2025
Revised manuscript received: July 07, 2025
Accepted manuscript online: July 08, 2025
Version of record online: July 16, 2025